

## New controlled rapid quench technique in a 1 atm infrared image furnace

MARK J. DAVIS\* AND PHILLIP D. IHINGER

Department of Geology and Geophysics, Yale University, New Haven, Connecticut 06511 U.S.A.

### ABSTRACT

We describe a new quench technique that allows for controlled and reproducible constant quench rates exceeding 100 °C/s in the temperature range of 1400–700 °C and ~10 °C/s in the range 1400–200 °C at 1 atm total pressure. Our technique uses a 1 atm infrared image furnace and a blower unit capable of discharging cooling air through the infrared furnace at speeds approaching 100 m/s. The control protocol consists of operating the furnace at a constant power setting, sufficient to reach the highest desired temperature, and modulating the blower output continuously; blower output is controlled via a silicon-controlled rectifier (SCR) using a proportional-integral-derivative (PID) algorithm on a personal computer (PC). A special autotuning procedure was used that enables the fine-tuning of PID parameters necessary for precise temperature control. Temperatures are controlled to  $\pm 1$  °C over the entire temperature range under isothermal conditions and to within 10 °C of the setpoint during quench. The range of accessible quench rates using our technique opens up new temperature-time paths for quantitative study. Potential applications include detailed studies on chemical diffusion and the kinetics of bubble and crystal formation under conditions of rapid temperature changes. Such studies have direct relevance to the crystallization, degassing, and structural relaxation of silicate melts during rapid temperature changes such as those encountered during volcanic eruptions.

### INTRODUCTION

Virtually all thermodynamic and kinetic properties of Earth materials are significantly affected by changes in temperature. A thorough understanding of the effect of temperature on various physical properties is an essential first step toward predicting the response of minerals, glasses, and melts to temperature-time ( $T-t$ ) paths found in nature. For example, detailed knowledge of how temperature affects kinetic properties of silicate melts better enables Earth scientists to (1) understand the physical processes that occur during rapidly changing  $T-t$  paths, such as those encountered during explosive volcanism; (2) estimate and even predict the amount of re-equilibration that occurs during quenches from high  $P-T$  experimental conditions, an important step toward successful interpretation of run results; and (3) achieve a deeper understanding of liquid dynamics through elucidation of structural changes caused by temperature changes of varying magnitude. Thus, a method for quenching experimental charges from high temperature at *controlled* rates would be a valuable addition to the range of techniques currently available to experimental petrologists. Current quench techniques for 1 atm furnaces, for example, generally produce either (1) controlled, but slow quench rates (<5 °C/s); or (2) uncontrolled, fast rates (up to 10<sup>3</sup> °C/s). We describe herein a 1 atm experimental setup capable of controlled and highly reproducible constant quench

rates exceeding 100 °C/s from temperatures as high as 1400 °C down to 700 °C; 50 °C/s quench rates can be maintained from 1400 to 400 °C. This enables experimentalists to quantitatively and reproducibly access a portion of  $T-t$  space previously unavailable.

### EXPERIMENTAL METHODS

The experimental setup used in this study is illustrated in Figures 1a and 1b. A Sinku-Riko infrared (IR) image furnace (model no. RHL-E45P) was used as the heat source. This furnace consists of four ~20 cm long “quartz”-tungsten lamps (actually silica glass, not quartz), each capable of producing 80 watts/cm<sup>2</sup> (W/cm<sup>2</sup>). The lamps are situated within gold-plated, parabolic reflecting surfaces machined into a water-cooled aluminum block. A 5 cm diameter fused silica tube (2 mm wall) was inserted into the furnace to protect the furnace lamps and reflective surfaces, as well as to provide for gas-mixing capabilities or operation under vacuum. Fused silica absorbs some of the energy emitted in the infrared, particularly for wavelengths longer than ~2.5 μm. However, since the radiative energy emitted by the hot tungsten element within the lamps must first pass through the silica tube that encloses each element, little additional energy is absorbed by the large silica tube used to protect the furnace. In addition, the IR energy is focused at the centerline of the furnace, not at the radial position of the large silica tube. Consequently, the large silica tube reaches temperatures considerably less than that of the sample.

\* E-mail: mark.davis@yale.edu

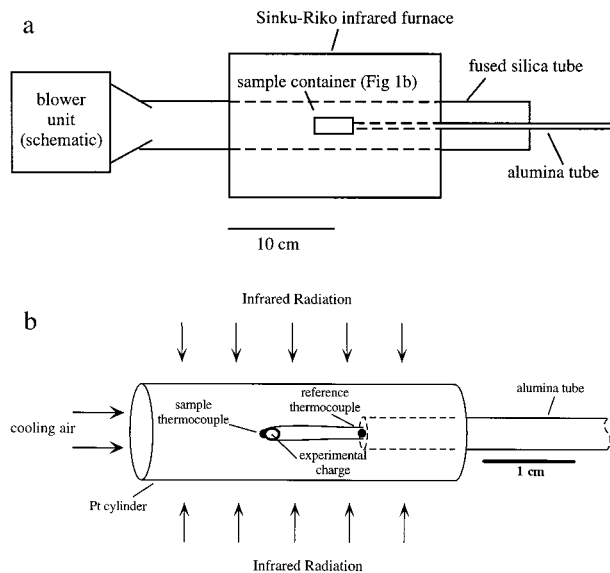


**FIGURE 1.** Cross-section of experimental setup used in this study: (a), view of IR furnace showing blower unit and position of sample; (b), detailed view of sample geometry. Note glass bead fused onto the thermocouple wire. Dimensions are appropriately scaled except for blower.

An external blower unit was situated at one end of the fused silica tube to facilitate rapid cooling. The blower unit, a 115 V, 1.1 kW Dayton “leaf-blower”, uses an electric fan to generate a maximum air flow rated at  $\sim 100$  liters/s with exhaust velocities approaching 100 m/s. The blower was connected to a phase-angle fired, silicon-controlled rectifier (SCR), which allowed for a continuous range of output from 0 to 100% power.

Sample geometry (Fig. 1) consisted of (1) a 0.64 cm dia. four-bore alumina tube with two sets of 0.5 mm dia.  $\text{Pt}_{94}\text{Rh}_6/\text{Pt}_{70}\text{Rh}_{30}$  thermocouple leads (one just exposed at the tip of the alumina rod, and another pulled  $\sim 1.5$  cm out from the tip); (2) a 3.5 cm-long platinum cylinder (1 cm dia., 0.33 mm wall thickness) attached to the alumina tube with platinum wire; and (3) the experimental charge attached to the well-exposed thermocouple lead. The platinum cylinder, although not essential, minimized the thermal gradients that existed in our IR furnace (see below). Moreover, because the platinum cylinder was open at both ends and cooling air travels lengthwise down the furnace, quench rates were not significantly affected by the presence of the platinum cylinder.

Various samples can be used with our setup, including minerals, glasses, and melts. The experiments reported below all used lithium disilicate ( $\text{Li}_2\text{Si}_2\text{O}_5$ ) glass as a starting material. Lithium disilicate was chosen because it is a well-characterized one-component, glass-forming silicate melt and exhibits a range of crystallization phenomena (James 1985; Davis and Ihinger 1998). We have carried out several studies using this material, including the effects of water and thermal history on crystal nucleation (Davis 1996; Davis et al. 1997), the process of hetero-

geneous crystal nucleation on bubbles (Davis and Ihinger 1998), and the influence of water on viscosity (Davis 1998, unpublished data) and structural relaxation (Davis and Ihinger 1998, unpublished data). All glasses were homogeneous with respect to both major elements (79.9 wt%  $\text{SiO}_2$ , 80.1 wt% nominal) and trace water contents ( $\sim 200$  ppm) (Davis et al. 1997).

We found that to achieve efficient heat transfer to the sample, as well as for accurate sample temperature measurements, the experimental charge required intimate contact with the thermocouple. This was achieved by bending the thermocouple wire around a  $\sim 2$  mm ( $\sim 20$  mg) glass cube prior to heating. Once melted, the sample assumed a roughly spherical shape, held to the wire by surface tension. Although the glass sample does absorb some of the radiation emitted by the lamps, a large portion of IR radiation is not absorbed due to the semi-transparent nature of glass in the IR region (see Gardon 1956 for relevant calculations). Heat is transferred via conduction from the hot wire to the glass sample.

Control of the sample temperature was achieved through the use of LabVIEW, a software package from National Instruments that allows users to monitor and control essentially any physical device using a PC. Data are stored directly to disk in spreadsheet format for later analysis. LabVIEW is not limited to any particular type of thermal program (i.e., linear ramps); for example, exponential or sinusoidal thermal histories are also achievable.

The most common technique used to control furnaces is the modulation of furnace power to minimize deviations of actual sample temperature from a desired setpoint temperature. This technique is most effective when isothermal operation is a priority. However, when controlled sample cooling rates over a range of quench rates are desired, relatively poor performance is often observed. One atmosphere furnaces are typically limited to quench rates of  $< 5$   $^\circ\text{C/s}$  to avoid damage to the ceramic tube used for atmosphere containment and because of the large thermal mass of the furnace. Even our IR furnace was incapable of cooling faster than  $\sim 30$   $^\circ\text{C}$  throughout a broad temperature range, due to the lack of an efficient means for removing the heat contained in the ceramic rod and platinum thermocouple assemblies (Figs. 1a and 1b). Drop quenches into a cooled liquid bath may be conducted with conventional 1 atm furnaces, thereby enabling far greater quench rates ( $\sim 10^3/\text{s}$ ), but they lack control or detailed knowledge of the  $T$ - $t$  path experienced by the sample. We thus incorporated a dedicated cooling device (blower) to increase the range of quench rates obtainable within our infrared furnace. Control of our IR furnace/blower system required a somewhat more sophisticated approach due to the presence of both heating and cooling units. In particular, there were two measured signals (sample and reference thermocouples) and two potential control variables (furnace and blower outputs). Due to large differences in heat transfer characteristics between the sample and reference thermocouples, large

temperature differences existed between them. In particular, the presence of the 4-bore alumina tube strongly influenced the temperature of the reference thermocouple due to the large thermal mass and radiative characteristics of our alumina tube. In addition, the sample thermocouple was more susceptible to the fan “wind” due to both its smaller mass and more exposed position in the furnace (Fig. 1b). Because of all these factors, the sample thermocouple commonly reached temperatures  $\sim 100$  °C less than the reference thermocouple. Thus, to obtain accurate temperature control, we used the sample thermocouple as the controlling signal. The reference TC could be used in a differential thermal analysis mode of operation, not investigated here.

The choice of control variables required considerable care. At first we tried to control the blower and furnace outputs simultaneously in what is known as selector control (Astrom and Hagglund 1995), which involves the implementation of uncoupled control loops for heating and cooling units. If the furnace alone can maintain temperature control during a programmed quench, then the cooling unit is not activated. Invariably, however, a lower temperature is reached at which control can no longer be maintained. At this point, the furnace is turned off and the cooling unit is activated and, in theory, the cooling unit then smoothly increases power to maintain temperature control. In practice, however (as we observed), the switch-over from heating control to cooling control is not smooth, and oscillations in temperature develop as the cooling unit is activated (Astrom and Hagglund 1995). We chose an alternative method that worked equally well in isothermal operation and rapid quench mode: Maintain the furnace at a constant power setting, sufficient to reach the highest desired temperature, while controlling the temperature entirely by controlling the power to the blower unit. This method involves a single-input/single-output control problem that is easily managed using standard control methods. As outlined below, our blower unit had sufficient power, sensitivity, and speed to control the sample temperature with great precision over a wide temperature range.

Control of the blower unit was obtained using the familiar PID algorithm (Astrom and Hagglund 1995). This algorithm monitors deviations of sample temperature from the setpoint (proportional,  $P$ ), the time accumulated during temperature deviations (integral,  $I$ ), and the time rate-of-change of temperature deviations (derivative,  $D$ ). The  $P$ ,  $I$ , and  $D$  parameters are task-specific and must be estimated carefully for optimum control. We wrote a LabVIEW “virtual instrument” (VI) that implements an autotuning algorithm based on relay feedback (Hang et al. 1993; Astrom and Hagglund 1995). Our algorithm optimized the control parameters by causing the blower to oscillate at its critical frequency by alternately increasing and decreasing power to the blower in predetermined amounts. Figure 2 shows the  $P$  parameter as a function of temperature for our experimental setup calculated using measured temperatures. In contrast to conventional

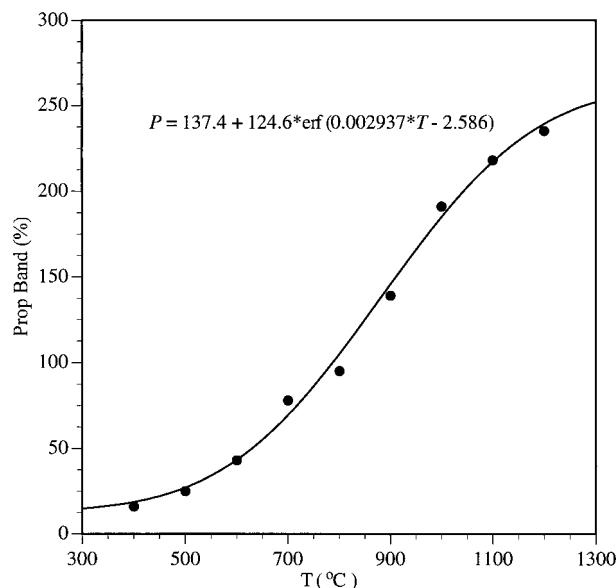


FIGURE 2. Proportional band ( $P$ ) of blower unit vs. sample temperature as measured in the IR furnace. Data were parameterized using the error function (equation and plotted curve).

electric resistance furnaces that show relatively little change in PID parameters with changes in temperature, our blower unit exhibits a strong dependence of  $P$  on temperature;  $P$  increases by over an order-of-magnitude (from  $\sim 10$  to 240%) with an increase in temperature from 400 to 1200 °C. In contrast,  $I$  and  $D$  were essentially temperature independent ( $I \approx 2.9$  s;  $D \approx 0.72$  s). We can compare performance to the best-fit PID parameters determined for temperature control achieved by adjusting power to the furnace (no blower present). In this case, the measured  $P$  was nearly temperature independent at  $\sim 25\%$ , but  $I$  was temperature dependent, decreasing from 25 s at 400 °C to 10 s at 1400 °C. Note that the blower was considerably more responsive than the furnace at all temperatures, indicated by substantially smaller  $I$  values, a measure of the time constant associated with the device. The larger values of  $P$  for blower control (for  $T > 600$  °C) implies that the blower unit was considerably more efficient at sample temperature control than the furnace, manifested as larger changes in temperature for a given change in applied power for the blower. At temperatures  $< 600$  °C the situation was reversed, where furnace control was more efficient than the blower.

The PID VI available from National Instruments was used as the control subroutine. A front-end VI was written by us to display setpoint, measured temperatures, and control parameters. Control was implemented at 10 Hz and provided measurably better control than when the control loop was operated at 1 Hz. The temperature dependence of  $P$  was directly introduced into the PID algorithm using the parameterized fit in Figure 2, a control technique known as gain scheduling in which non-con-

stant control parameters are allowed (Astrom and Haglund 1995).

To calibrate temperatures in our IR image furnace when temperatures were controlled by the blower, a series of melting point determinations were made in which crystalline lithium disilicate, obtained by crystallizing a lithium disilicate glass sample at  $\sim 750$  °C for 10 min, was heated to various temperatures for  $\sim 5$  min. Our melting point determinations were about 10 °C higher than the accepted value of 1034 °C (Kracek 1930). In particular, visual inspection of the sample at high temperature revealed that when the sample thermocouple read  $\sim 1044$  °C, the sample bead was partially crystalline with the portion nearest to the thermocouple bead fully melted. By  $\sim 1048$  °C the sample was completely melted. This suggests the sample experiences a temperature gradient of  $\sim 10$  °C at steady-state heat flow conditions. This gradient could be decreased if smaller experimental charges were used. However, as  $dT/dt$  is important during quenches and not  $T$  alone, a small thermal gradient in the sample should not lead to a large uncertainty in measured quench rates. Moreover, we argue below that our  $T-t$  data indicate that strongly non-isothermal conditions did not exist for even our highest quench-rate experiments, suggesting that gradients were never much larger than 10 °C.

Radial temperature gradients within the furnace were measured by moving the sample holder assembly, with and without the platinum cylinder enclosing the sample. These measurements were made with the blower unit off and the furnace set at a pre-designated constant power setting. With the sample assembly placed along the centerline of the furnace, we found the sample temperature was independent of the presence or absence of the platinum cylinder surrounding the sample. However, when the sample was displaced radially 0.5 cm from the centerline, large temperature differences were found depending on whether the platinum cylinder was present or absent. In particular, at a furnace center temperature of 1100 °C, a drop of  $\sim 90$  °C was observed without the platinum cylinder, but only  $\sim 30$  °C with it. At a furnace center temperature of 1175 °C, the differences were magnified: A drop of  $\sim 140$  °C was observed without the platinum cylinder and only  $\sim 45$  °C with it.

Longitudinal temperature gradients are reported by the manufacturer and show a nearly constant temperature region  $\pm 3$  cm from the longitudinal midpoint; we verified this using our experimental setup illustrated in Figure 1. Because our platinum cylinder was contained entirely within the region of constant temperature, we expect negligible longitudinal temperature gradients. We emphasize that even with the large measured radial temperature gradients, the high level of control we have over sample temperature and the strong physical connection between thermocouple and sample lessens the importance of thermal gradients within our IR furnace.

## RESULTS AND DISCUSSION

For physical processes limited by kinetics (e.g., diffusion), the relevant measure of intensive variables is not

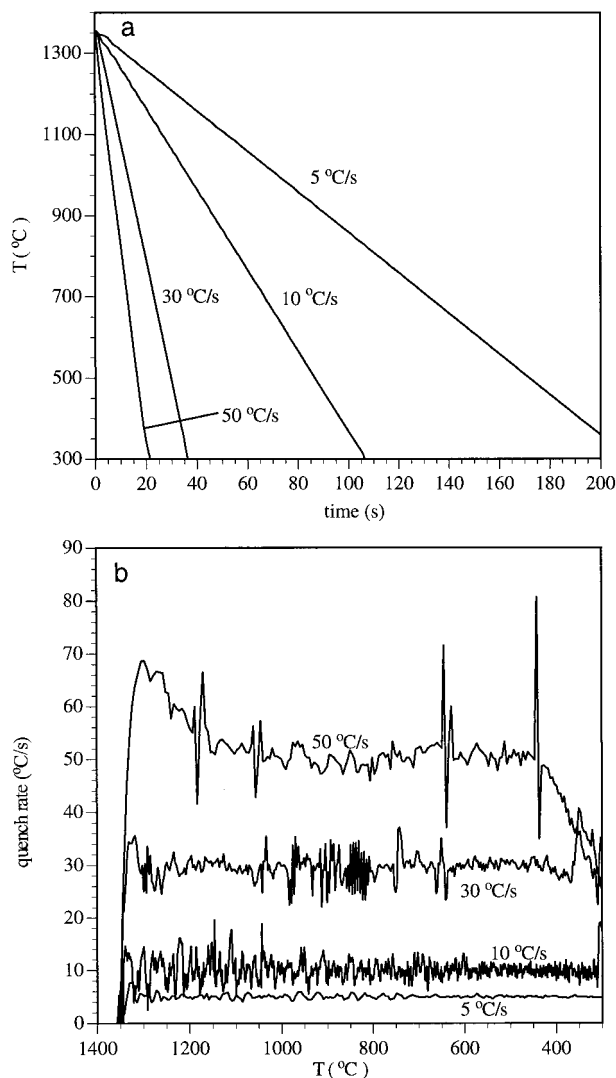


**FIGURE 3.** Selected thermal histories obtained using the IR furnace and blower unit. (a) measured  $T-t$  paths for four quench rates. (b) measured  $dT/dt-T$  paths for same thermal histories as in (a); temperature derivatives were calculated from measured values using simple first-order finite differences:  $dT/dt \sim \Delta T/\Delta t$ . Note good agreement of measured quench rate with programmed rate, particularly for quench rates  $< 50$  °C/s. The 50 °C/s quench exhibits an initial overshoot in rate until  $\sim 1150$  °C, followed by a nearly 700 °C drop in temperature at almost precisely 50 °C/s until  $\sim 500$  °C, at which point the blower unit reached maximum capacity (see text).

only their absolute values but also their rate of change with time. Thermal history data are typically viewed on plots of  $T$  vs.  $t$  or  $dT/dt$  vs.  $T$ .  $T-t$  plots offer the advantage of illustrating thermal histories in a straightforward manner whereas  $dT/dt-T$  plots allow for an immediate evaluation of the rate of cooling or heating at any particular temperature. Our experimental technique allows for simultaneous characterization of  $T$  and  $dT/dt$  as functions of time. Figure 3a shows measured  $T-t$  paths for various

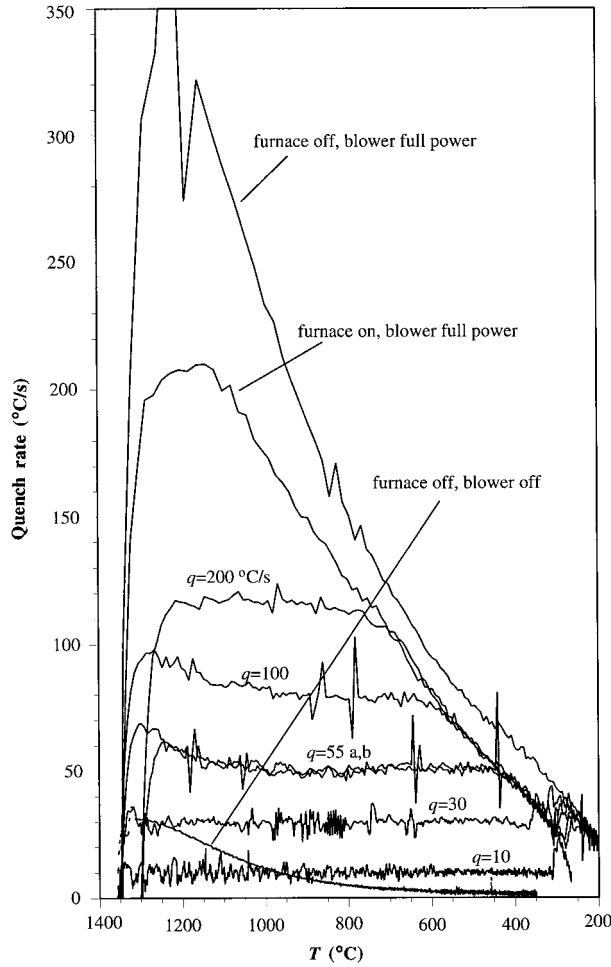


FIGURE 4. Quench rate vs. temperature showing selected thermal histories. Curves are labeled with either programmed quench rate  $q$  ( $^{\circ}\text{C}/\text{s}$ ) or status of furnace and blower during thermal program.

constant quench rates used in cooling an experimental charge from 1350 to 300  $^{\circ}\text{C}$ . Figure 3b shows the measured instantaneous quench rate as a function of temperature ( $dT/dt$  vs.  $T$ ). The noise in the calculated temperature derivatives is due to taking small differences between large numbers (temperatures) that are themselves subject to low-level electrical noise. Only the 50  $^{\circ}\text{C}/\text{s}$  quench rate deviates noticeably from the desired rate, and does so only at temperatures below 500  $^{\circ}\text{C}$  or above 1200  $^{\circ}\text{C}$ .

The range of thermal histories accessible with our experimental technique is illustrated in Figure 4. First, we note the existence of two similar curves, one labeled “furnace on, blower full power” and the other “furnace off, blower full power.” These refer to maximum cooling rates obtained with and without the furnace operating, respectively, achieved by instantly turning the blower on to full power at high temperature (1350  $^{\circ}\text{C}$ ). Both  $dT/dt$ - $T$  paths exhibited a very rapid increase to maximum quench rates ( $\sim 200$   $^{\circ}\text{C}/\text{s}$  with the furnace on,  $\sim 350$   $^{\circ}\text{C}/\text{s}$

with it off). The maximum quench rate was followed in both cases by a nearly linear decrease in quench rate with decreasing temperature, particularly for temperatures  $< 800$   $^{\circ}\text{C}$  (Fig. 4), indicating that the instantaneous sample quench rate decreased exponentially with time. This is the expected behavior for the cooling of an isothermal body with a nearly constant heat transfer coefficient (Incropera and DeWitt 1990). In contrast, note that the curve for the “furnace off, blower off” case exhibits a non-linear cooling rate path, probably due to the pronounced effect of strongly temperature-dependent radiative cooling predominating at high temperature in the absence of forced convection. In addition, the maximum cooling rate in the “blower off” case is nearly 10 times less than that obtained with the blower on full, illustrating the efficiency with which forced convection can affect heat transfer.

We can verify that an exponentially decreasing quench rate is the expected behavior for a system cooled largely via forced convection through consideration of energy conservation. Assuming for the moment that our samples were nearly isothermal (to be verified *a posteriori*), the appropriate energy conservation equation for our experimental setup has no spatial dependence (Incropera and DeWitt 1990):

$$-hA(T - T_{\infty}) = \rho VC_p \frac{dT}{dt} \quad (1)$$

where  $h$  is the heat transfer coefficient ( $\text{W}/\text{m}^2/\text{K}$ ), and  $A$ ,  $V$ ,  $\rho$ , and  $C_p$  are surface area, volume, density, and specific heat, respectively, of the isothermal body (our glass beads are approximated as spheres) and  $T_{\infty}$  is the far-field temperature (25  $^{\circ}\text{C}$ ). Note that Equation 1 predicts that  $dT/dt$  is proportional to  $T$  (in agreement with Figure 4), if  $h$  has, at most, a weak dependence on temperature. If the heat transfer coefficient is assumed to be temperature-independent and, neglecting the small temperature dependence for  $\rho$  and  $C_p$  of the sphere (estimated at  $< 3\%$ ; Shartsis et al 1952; Richet and Neuville 1992), Equation 1 can be integrated directly to give:

$$\frac{T - T_{\infty}}{T_i - T_{\infty}} = \exp\left[-\left(\frac{hA}{\rho VC_p}\right)t\right] \quad (2)$$

where  $T_i$  is the initial temperature of the sphere. The temperature dependence of the heat transfer coefficient can be estimated using the correlation due to Whitaker (1992) that gives the Nusselt number for forced convection [the Nusselt number is the ratio of actual heat transfer across a surface to that due only to conduction (Rosner 1986)]:

$$\overline{Nu}_d = 2 + (0.4Re_d^{1/2} + 0.06Re_d^{2/3})Pr^{0.4}\left(\frac{\mu}{\mu_s}\right) \quad (3)$$

where

$$Re_d = \frac{Vd}{\nu} \quad (4)$$

$\overline{Nu}_d$  is the surface-averaged Nusselt number based on the diameter of the sphere,  $d$ ,  $Re_d$  is the Reynolds number,  $Pr$

is the Prandtl number, and  $\nu$  and  $\mu$  are the kinematic and dynamic viscosities, respectively, of air. The subscript  $s$  refers to the value of  $\mu$  evaluated at the sphere temperature; all other parameters are evaluated at the far-field temperature.

To obtain the heat transfer coefficient one uses the relation:

$$h = \frac{\overline{Nu}_s k}{d}, \quad (5)$$

where  $k$  is thermal conductivity of the air. Numerical evaluation of Equations 3, 4, and 5 reveals that even for an extreme air velocity of 100 m/s,  $h$  decreases by only ~12% (from 1055 to 926 W/m<sup>2</sup>/K) with an increase in temperature from 400 to 1400 °C [values for the relevant physical parameters for air taken from Incropera and DeWitt (1990)]. This small change in  $h$  with temperature suggests that the observed exponentially decaying rate of cooling (Fig. 4) is most likely due to near isothermal conditions in the sphere (Eq. 2).

Further support for our neglect of thermal gradients within the cooling sample comes from consideration of the Biot number ( $Bi$ ), defined as the ratio of the resistance of heat loss due to a finite rate of conduction within the sphere, to the resistance arising from finite heat loss into the surrounding air (Rosner 1986):

$$Bi = \frac{hL}{k} \quad (6)$$

where  $L$  is a characteristic length scale (radius/3, for a sphere) and  $k$  is the thermal conductivity of the glass bead [e.g.,  $k = 0.88$  W/m/K for lithium disilicate (Ammar et al. 1983) and 1.59 W/m/K for rhyolite (Bagdassarov and Dingwell 1994)]. Based on literature values for  $k$  and a maximum estimate for heat transfer noted above (~1000 W/m<sup>2</sup>/K, maximum), we calculate a Biot number of ~0.4 for lithium disilicate at an air velocity of 100 m/s; at an air velocity of 10 m/s,  $h$  decreases to ~300 W/m<sup>2</sup>/K and  $Bi$  decreases to ~0.1. Generally, when  $Bi < 0.1$ , thermal gradients within a cooling body can be neglected for most purposes (Incropera and DeWitt 1990). It is likely, therefore, that nearly isothermal conditions would exist in the cooling sample, with the exception of the highest quench rates that involve very high air velocities. However, simply decreasing the size of the sample could significantly lessen thermal gradients, as evident in Equation 6. In addition, there is a weak dependence of thermal conductivity on composition that should be taken into account; using  $k$  values for rhyolite instead of those for lithium disilicate in the above calculations, we obtain  $Bi$  values of 0.2 and 0.06 for air velocities of 100 and 10 m/s, respectively. Thus, geologically relevant materials are even more likely to maintain isothermal conditions during the rapid quenching achieved with our technique.

The region within the “furnace off, blower full power” curve (Fig. 4) represents the range of  $T-t$  paths accessible with our technique. Curves in Figure 4 are labeled with the quench rates that the controller attempted to maintain.

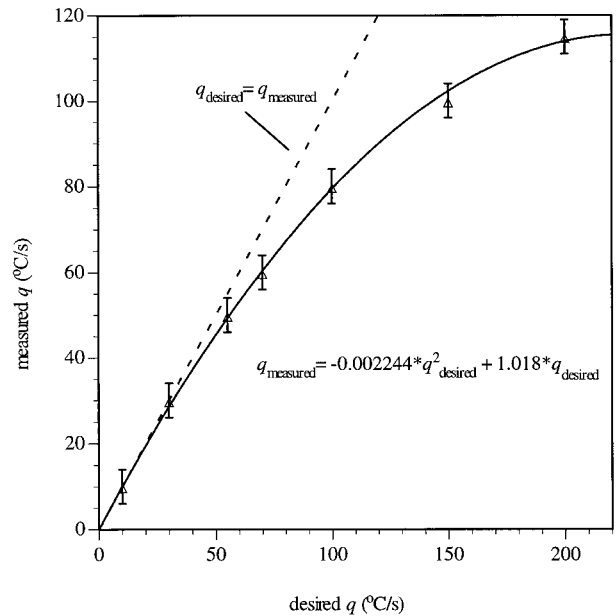


FIGURE 5. Summary of measured quench rates vs. programmed quench rates; data parameterized with a quadratic equation with zero intercept. Error bars on quench rates were estimated based on noise in computed derivatives.

Curves labeled  $q = 55a$  and  $55b$  are identical except for their initial temperatures, one being 1300 °C and the other 1350 °C. However, notice that very quickly they follow the identical  $dT/dt$  path, indicating no dependence on thermal history (i.e., no memory effect). Note that in all cases a constant quench rate is obtained at temperatures within ~150 °C of the initial temperature. The region of constant quench rate extends down temperature to the intersection of the particular quench path with the “furnace on, blower full power” curve. At this point, the blower power was at 100%, and the sample then experienced the same  $dT/dt$  path as the “furnace on, blower full power” path, again indicating no memory effect. Thus the “furnace on, blower full power” path represents an envelope of quench rates, within which we have freedom to obtain the quench rate we desire. The “furnace off, blower full power” condition describes a different envelope (outermost curve in Fig. 4). Shutting off power to the furnace results in a shift of the  $T-t$  path to the outermost envelope. For example, at very low temperatures (~300 °C), some of the measured paths cross over to the “furnace off, blower full power” curve. At the point of departure from the “furnace on, blower full power” path, the furnace was shut off; the  $dT/dt-T$  path then jumped to the outermost, furnace-off, envelope. Note also that the difference in quench rate for the furnace-on/furnace-off curves is only ~15 °C/s at temperatures less than ~800 °C, again demonstrating the power of the blower unit to cool our samples.

The measured quench rate did not always correspond to the programmed quench rate (Fig. 4). Figure 5 plots

measured quench rates, given by the horizontal portions of the  $dT/dt$ - $T$  curves in Figure 4, vs. the desired quench rate. For quench rates  $<50$  °C/s, there is nearly perfect correspondence between desired and measured quench rates; at higher quench rates a significant deviation is observed. For example, a desired quench rate of 200 °C/s resulted in a measured rate of  $\sim 115$  °C/s. We believe that the deviation from desired behavior is due to the sample assembly being out of thermal equilibrium with its surroundings. The PID parameters obtained using our auto-tuning method are strictly correct only if the furnace assembly is at or near steady-state heat flow conditions. During rapid cooling, this is clearly not the case. We believe it was the large temperature dependence of the control parameter  $P$  that resulted in relatively poor control at high quench rates. If  $P$  was temperature independent, we would expect better performance at high quench rates. One solution, not attempted here, is to allow  $P$  to depend not only on  $T$ , but on  $dT/dt$ . However, the systematic deviation in quench rates (Fig. 5) allows us to obtain our desired  $dT/dt$  simply by using the fit derived from the data in Figure 5. This approach was used successfully by Davis and Ihinger (1998, unpublished data) in their study of the effect of thermal history on crystal nucleation.

There are various applications that could benefit from the ability to induce rapid yet controlled changes in temperature under high-temperature conditions at 1 atm total pressure. Two such applications are outlined below, which illustrates the ability of our technique to increase the range of experimental conditions currently accessible to experimental petrology.

### Volcanic eruption

A considerable effort has been focused recently on understanding magma degassing and crystallization under near surface conditions, particularly for eruptive events (e.g., Sparks 1978; Cashman 1992; Mangan et al. 1993). The time scales associated with explosive volcanic eruptions, in which pyroclastic material is ejected into air, roughly corresponds with the cooling rates obtainable in our apparatus. Processes including crystallization and phenomena associated with the glass transition in silicate melts can now be examined for controlled quench rates exceeding 100 °C/s. Due to the flexibility of software-driven furnace control, such as that reported in this study, complex experimental  $T$ - $t$  paths can be prescribed to mimic natural thermal histories of eruptions.

### Cation ordering kinetics

A recently described "geospeedometer," based on cation ordering in olivine (Redfern et al. 1996), underscores the need for accurate calibration of the quench-rate dependence of various physical parameters. Redfern et al. (1996) deduced cooling rates of natural samples using an

experimentally calibrated kinetic model of metal-cation ordering. Our experimental setup will now allow such calibrations to include data obtained from experiments with well-characterized quench rates exceeding 100 °C/s.

### ACKNOWLEDGMENTS

The authors thank G. Ulmer, J. Ayers, and D. Jenkins for insightful reviews. This work has been supported by a generous grant from the Packard Foundation.

### REFERENCES CITED

- Ammar, M.M., Gharib, S.A., Halawa, M.M., El-Batal, H.A., and El-Badry, K. (1983) Thermal conductivity of silicate and borate glasses. *Journal of the American Ceramic Society*, 66, C76-C77.
- Astrom, K.J. and Hagglund, T. (1995) *PID Controllers: Theory, Design, and Tuning*, 343 p. The International Society for Measurement and Control, North Carolina.
- Bagdassarov, N. and Dingwell, D. (1994) Thermal properties of vesicular rhyolite. *Journal of Volcanology and Geothermal Research*, 60, 179-191.
- Cashman, K.V. (1992) Groundmass crystallization of Mount St. Helens dacite, 1980-1986: a tool for interpreting shallow magmatic processes. *Contributions to Mineralogy and Petrology*, 109, 431-449.
- Davis, M.J. (1996) Influence of water and thermal history on viscosity and nucleation kinetics of lithium disilicate melt. *Geology and Geophysics*, p. 159. Ph.D. thesis, Yale University, New Haven, Connecticut.
- Davis, M.J. and Ihinger, P.D. (1998) Heterogeneous crystal nucleation on bubbles in silicate melt. *American Mineralogist*, 83, 1008-1015.
- Davis, M.J., Ihinger, P.D., and Lasaga, A.C. (1997) Influence of water on nucleation kinetics in silicate melt. *Journal of Non-Crystalline Solids*, 219, 62-69.
- Gardon, R. (1956) The emissivity of transparent materials. *Journal of the American Ceramic Society*, 39, 278-287.
- Hang, C.C., Lee, T.H., and Ho, W.K. (1993) *Adaptive Control*, 261 p. Instrument Society of America, North Carolina.
- Incropera, F.P. and DeWitt, D.P. (1990) *Introduction to heat transfer*, 824 p. Wiley, New York.
- James, P.F. (1985) Kinetics of crystal nucleation in silicate glasses. *Journal of Non-Crystalline Solids*, 73, 517-540.
- Kracek, F.C. (1930) The binary system  $\text{Li}_2\text{O-SiO}_2$ . *Journal of Physical Chemistry*, 34, 2641-2650.
- Mangan, M.T., Cashman, K.V., and Newman, S. (1993) Vesiculation of basaltic magma during eruption. *Geology*, 21, 157-160.
- Redfern, S.A.T., Henderson, C.M.B., Wood, B.J., Harrison, R.J., and Knight, K.S. (1996) Determination of olivine cooling rates from metal-cation ordering. *Nature*, 381, 407-409.
- Richet, P. and Neuville, D.R. (1992) Thermodynamics of silicate melts: configurational properties. In S.K. Saxena, Ed., *Advances in Physical Geochemistry*, 10, p. 367. Springer Verlag, New York.
- Rosner, D.E. (1986) *Transport Processes in Chemically Reacting Flow Systems*, 540 p. Butterworth-Heinemann, Boston, Massachusetts.
- Shartsis, L., Spinner, S., and Capps, W. (1952) Density, expansivity, and viscosity of molten alkali silicates. *Journal of the American Ceramic Society*, 35, 155-160.
- Sparks, R.S.J. (1978) The dynamics of bubble formation and growth in magmas: A review and analysis. *Journal of Volcanology and Geothermal Research*, 3, 1-37.
- Whitaker, S. (1972) Forced convection heat transfer correlations for flow in pipes, past flat plates, single cylinders, single spheres, and for flow in packed beds and tube bundles. *American Institute of Chemical Engineering Journal*, 18, 361-371.

MANUSCRIPT RECEIVED DECEMBER 22, 1997

MANUSCRIPT ACCEPTED AUGUST 14, 1998

PAPER HANDLED BY DAVID JENKINS